IJCRT.ORG ISSN : 2320-2882

INTERNATIONAL JOURNAL OF CREATIVE RESEARCH THOUGHTS (IJCRT)

An International Open Access, Peer-reviewed, Refereed Journal

# Optical properties of $Fe_2O_3$ and $Fe_2O_3$:Dy/Eu nanocrystalline films prepared by SILAR method

[1]Rukhmani Rai, [2]Mina Mishra, [3]Sandhya Pillai

[1]M.tech scholar, [2]Head of Department, [3]Head of Department

*[1]Department of Nanotechnology*

*[1]Christian College of Engineering and Technology, Kailash Nagar, Bhilai-490026, Chhattisgarh, India*

***Abstract:*** Undoped and Dy/ Eu doped $Fe_2O_3$ thin films were deposited onto glass substrates using SILAR method. The films were prepared at 60 SILAR cycles and further annealed at 300°C. The optical properties of the films were investigated using optical absorption spectra and optical constants were determined and their variation was plotted against wavelength. The direct band gap energy values were determined using Tauc's plots and were found to be in the range of 2.95eV to 3.15eV. Lower absorbance is observed in doped films in comparison to the un-doped $Fe_2O_3$ films. However the band gap values of doped films are higher than the un-doped films. On annealing, the band gap values were found to decrease. The optical constants were found to have higher values at lower wavelengths and were constant in the visible region of the spectrum.

***Keywords*: SILAR method, Absorption, XRD, optical, SEM, EDX, Optoelectronic.**

## *I. Introduction*

Nanomaterials have gained importance in recent years due to their unique structural, optical, electronic, magnetic and chemical properties which can be tuned by manipulating their size during growth. Nanocrystalline binary metal oxide semiconductors have demonstrated themselves as viable materials for optoelectronic devices and has become a rapidly growing area of research[1-4]. n- type α-$Fe_2O_3$ (Hematite) has attracted lot of attention as they find wide applications in sensors, supercapacitors, solar cells, solar filters etc [5-9]. However, the efficiency of α-$Fe_2O_3$ in optoelectronic applications is affected due to fast recombination of photo generated electrons and holes. It has been reported that doping of α-$Fe_2O_3$ with transition metals and rare-earth ions result in lowering the electron hole recombination and in band gap tailoring [10-13]. Rare-earth elements have the ability to release trivalent cat-ions due to their f-electronic configuration which in turn changes the structure and the optical properties of the host material [14, 15]. In the present work, α-$Fe_2O_3$ has been doped with rare earth elements ($Dy^{3+}$/$Eu^{3+}$) (not reported earlier) and its effect on the optical properties of α-$Fe_2O_3$ has been studied.

Several physical and chemical methods have been used to deposit α-$Fe_2O_3$ thin films such as electro-deposition, spray pyrolysis, atomic layer deposition, radio frequency magnetron sputtering, Metal organic chemical vapor deposition, atmospheric pressure chemical vapor deposition, plasma-enhanced chemical vapor deposition, aqueous combustion method, sol-gel and successive ionic layer adsorption and reaction (SILAR) methods [5, 16-18]. SILAR method has become increasingly popular technique in growing nanocrystalline films as it is simple, non hazardous and economically viable. The method involves immersion of the substrate into cationic and an-ionic precursors alternately. The substrate is rinsed with the de- ionized water to remove the loosely bound particles to get an adherent film. The growth is controlled by altering the number of deposition cycles. The present paper reports the synthesis of un-doped and Dy/Eu doped α-$Fe_2O_3$ films by SILAR method for 60 cycles. The effect of Dy and Eu dopant on the optical properties of $Fe_2O_3$ films was studied. The films were also annealed at 300℃ and the properties of the un-annealed and annealed films were investigated. The optical Constants of the films were also determined from the absorption spectral studies.

## *II.* Experimental Techniques

### 2.1 Preparation of un-doped and Dy doped α-$Fe_2O_3$ thin films.

The nanocrystalline α- $Fe_2O_3$ thin films were deposited by SILAR method onto glass substrates. For the deposition of thin films, 0.05mol/L Ferric chloride was used as a cationic precursor and 0.05 mol/L sodium hydroxide was used as the anionic precursor. In the case of doped films, 0.05M solution of $Dy_2O_3$ and 0.05M solution of $Eu_2O_3$ were mixed with the cationic precursor.

Before deposition, glass substrates were washed and cleaned with de-ionized water and then immersed in a cationic precursor solution for 20sec for the adsorption of iron species on the substrate surface. The substrate was then rinsed in de-ionized water for 20sec to remove weakly bound species of $Fe^{3+}$ ions from its surface. The substrate was then immersed in an anionic precursor NaOH for 20sec to form a layer of iron oxide material. To remove un-reacted and excess species from substrate, it was rinsed in de-ionized water for 20sec. This completes one SILAR cycle. By repeating such sixty SILAR cycles, brown colored, uniform thin film of $Fe_2O_3$ was obtained. In the doped films, 2ml of $Dy_2O_3$/$Eu_2O_3$ solution was mixed with $FeCl_3$ before starting the SILAR cycles. After deposition, the films were dried at room temperature and then annealed at 300℃ in a muffle furnace.

### 2.2 Absorption Spectral Studies:

The optical absorption spectra of the un-annealed and annealed pure $Fe_2O_3$ and $Fe_2O_3$: Dy/Eu films are shown in Fig 1 (a) and (b) respectively. The absorption edge in the case of both un- annealed and annealed pure and doped $Fe_2O_3$ films is around 380nm. The absorbance is less in the case of Dy/Eu doped films in comparison to pure $Fe_2O_3$ films.

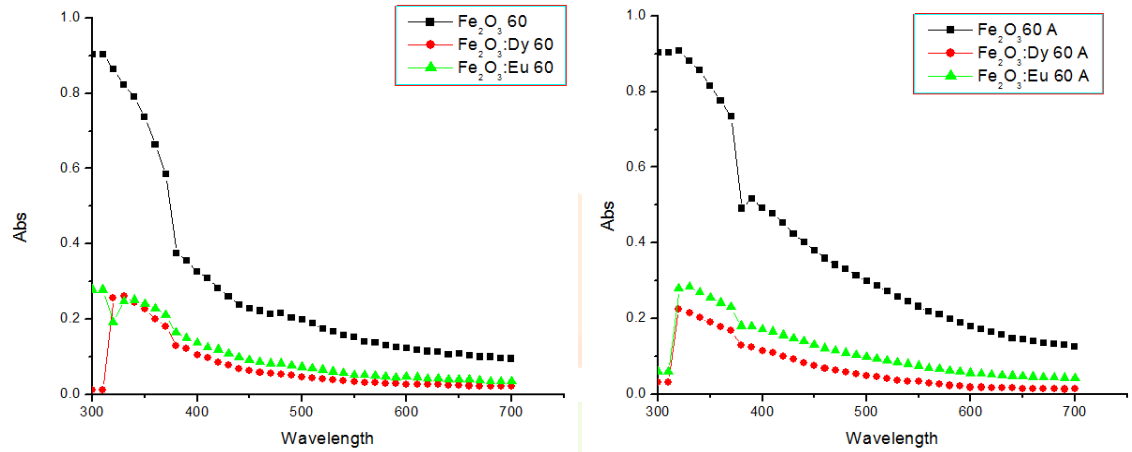


**(a) un-annnealed** **(b) annealed**

Fig 1 (a) and (b) - Absorption spectra of $Fe_2O_3$ and $Fe_2O_3$:Dy/Eu un-annealed and annealed thin film prepared by SILAR method at 60 SILAR cycles.

The optical absorption coefficient α and band gap Eg (for direct band gap materials) are represented by the equation

$$\alpha = c(hv - Eg)^{1/2}/hv \quad \ldots\ldots\ldots\ldots\ldots\ldots\ldots\ldots\ldots\ldots (1)$$

Where Eg is the optical band gap and c is the constant. Thus a plot between $(\alpha hv)^2$ vs hv (Tauc's plot) gives the band gap value Eg of the corresponding material. The Tauc's plots of the un-annealed and annealed pure $Fe_2O_3$ and $Fe_2O_3$: Dy/Eu films are shown in fig 2 (a) and (b) respectively and the corresponding band gap values are presented in table 1. It can be observed from the table that the band gap values of the Dy and Eu doped films are higher than pure $Fe_2O_3$ in both un- annealed and annealed films. Also the band gaps of the annealed films are lower than the un-annealed films. The optical band gap energies of the $Fe_2O_3$ films are in good agreement with the reported results. [19-21]

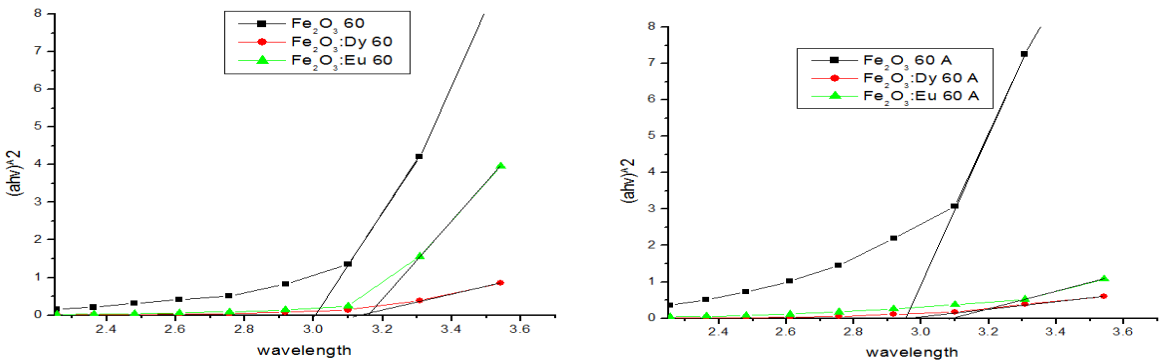


**(a) Un- annealed** **(b) annealed**

Fig 2 (a) and (b) - Tauc's plot of $Fe_2O_3$ and $Fe_2O_3$: Dy un-annealed and annealed thin films prepared by SILAR method 60 SILAR cycle.

Table 4:- Optical band gaps of the pure and doped $Fe_2O_3$ films:

| Sample Name | Band gap (eV) | |
|---|---|---|
| | Un-annealed | Annealed |
| $Fe_2O_3$ | 2.98 | 2.95 |
| $Fe_2O_3$: Dy | 3.13 | 2.99 |
| $Fe_2O_3$ :Eu | 3.15 | 3.09 |

**2.3 Determination of Optical Constants:-**

There are several quantities known as optical constants which are characteristic of the optical behavior of a substance like refractive index, extinction coefficient, dielectric constants etc. Optical Absorption and transmittance spectra are very useful in the determination of these constants.

2.3.1 Refractive Index

Refractive index (n) is a fundamental property of an optical material as it provides the information about the interaction of light and nanoparticles and hence is of importance to our health and environment. Evaluation of the refractive index of these materials is important for application in various integrated optical devices.

In the present work the refractive indices were determined by Envelope method proposed by Swanepoel [22]. For energies greater than band gap or for free carrier absorption at higher wavelength, the dispersion of n and k is not very large [23]. Using the Envelope method, the refractive index of the film on a transparent substance can be evaluated from the transmittance spectra using the relation.

$$n = \sqrt{N + \sqrt{(N^2 - ns^2)}} \quad \ldots\ldots\ldots\ldots\ldots\ldots (2)$$

$$N = \frac{(ns^2+1)}{2} + 2ns\frac{TM-Tm}{TM\,Tm} \quad \ldots\ldots\ldots\ldots\ldots\ldots (3)$$

and $n_s$ is the refractive index of the substrate ($n_s$=1.52 for glass)

Figures 3.(a) and (b) show the variation of Refractive Index with wavelength of $Fe_2O_3$, $Fe_2O_3$ : Dy and $Fe_2O_3$ : Eu at 60 SILAR cycles for un-annealed and annealed films.

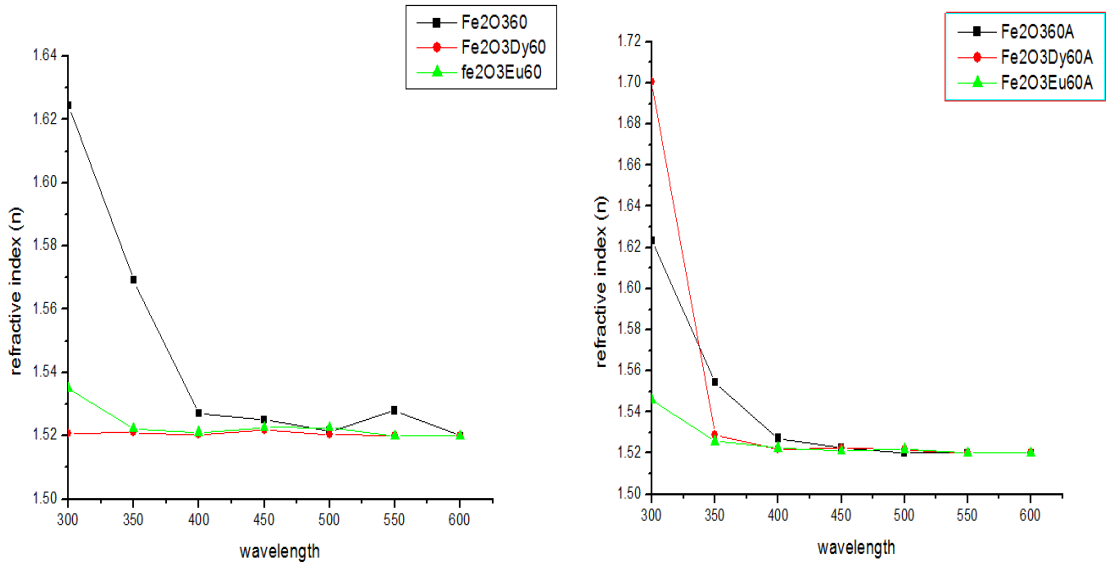


(a) un-annealed (b)annealed

Fig 3 (a) and (b)- Refractive index of $Fe_2O_3$ , $Fe_2O_3$ : Dy/Eu for 60 SILAR cycle on un-annealed and annealed film.

It can be observed that the values of refractive index are higher at lower wavelengths and is seen to decrease and becomes a constant in the visible region.

**2.3.2 Extinction Coefficient:-**

The extinction coefficient is calculated from eq. (4) and (5)

$$k = \frac{\alpha\lambda}{4\pi} \quad \text{..... (4)}$$

$$\alpha = \frac{2.303\ A}{d} \quad \text{..... (5)}$$

Where α is the absorption coefficient and d is the film thickness.

Figures 4 (a) and (b) show the variation of Extinction Coefficient with wavelength of $Fe_2O_3$, $Fe_2O_3$ : Dy and $Fe_2O_3$ : Eu at 60 SILAR cycles for un-annealed and annealed films.

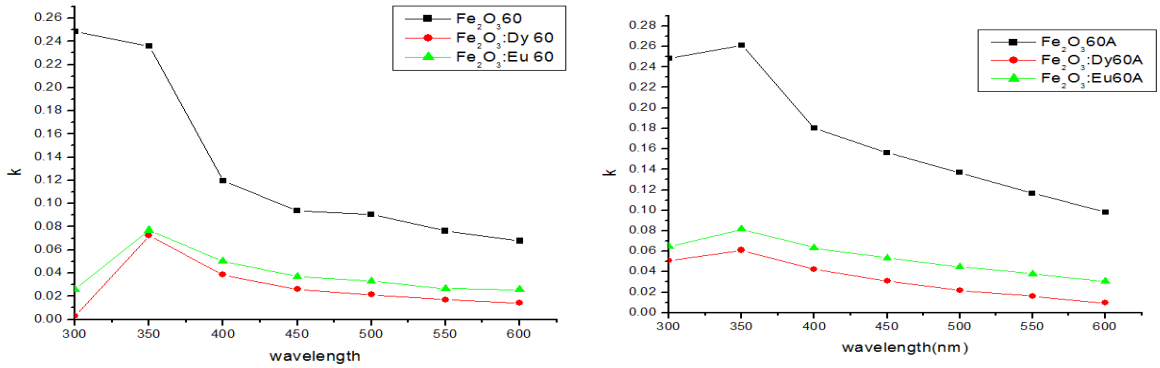


(a) un-annealed (b) annealed

Fig 4 (a) and (b) - Extinction coefficient of $Fe_2O_3$ , $Fe_2O_3$ : Dy and $Fe_2O_3$ : Eu for 60 SILAR cycle on un-annealed and annealed film.

A similar behavior is seen in this case also as observed for the variation of refractive index. The values of extinction coefficient also is higher at lower wavelengths and is almost constant in the visible region.

### 2.3.3 Optical Conductivity:-

Figures 5 (a) and (b) show the variation of optical conductivity with wavelength of $Fe_2O_3$, $Fe_2O_3$ : Dy and $Fe_2O_3$ : Eu at 60 SILAR cycles for un-annealed and annealed films.

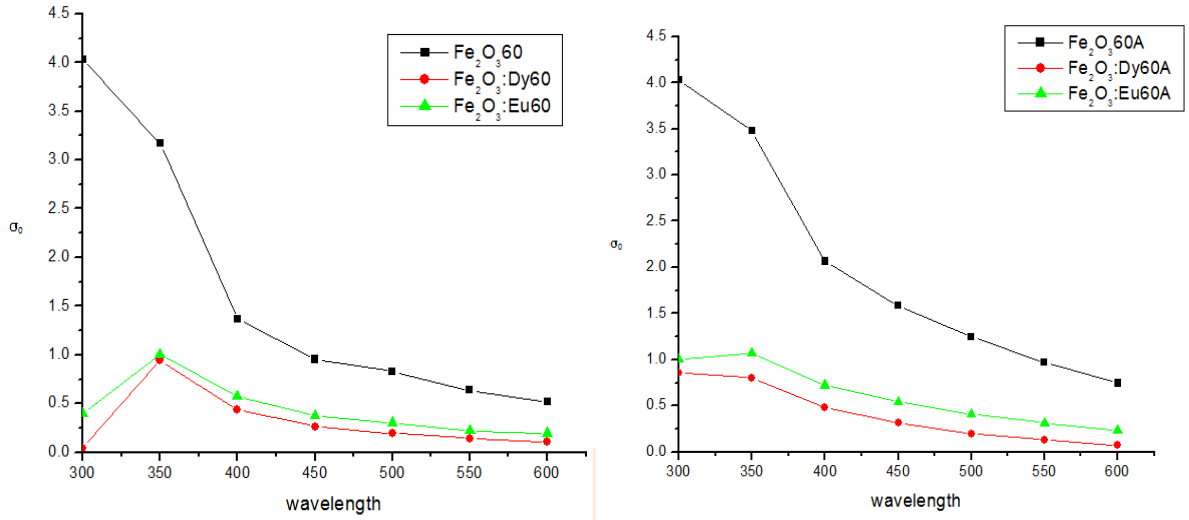


(a) un-annealed (b) annealed

Fig 5(a) and (b) - Optical Conductivity of $Fe_2O_3$ , $Fe_2O_3$ : Dy and $Fe_2O_3$ : Eu for 60 SILAR cycle on un-annealed and annealed film.

### 2.3.4 Electrical Conductivity:-

Figures 6 (a) and (b) show the variation of electrical conductivity with wavelength of $Fe_2O_3$, $Fe_2O_3$ : Dy and $Fe_2O_3$ : Eu at 60 SILAR cycles for un-annealed and annealed films.

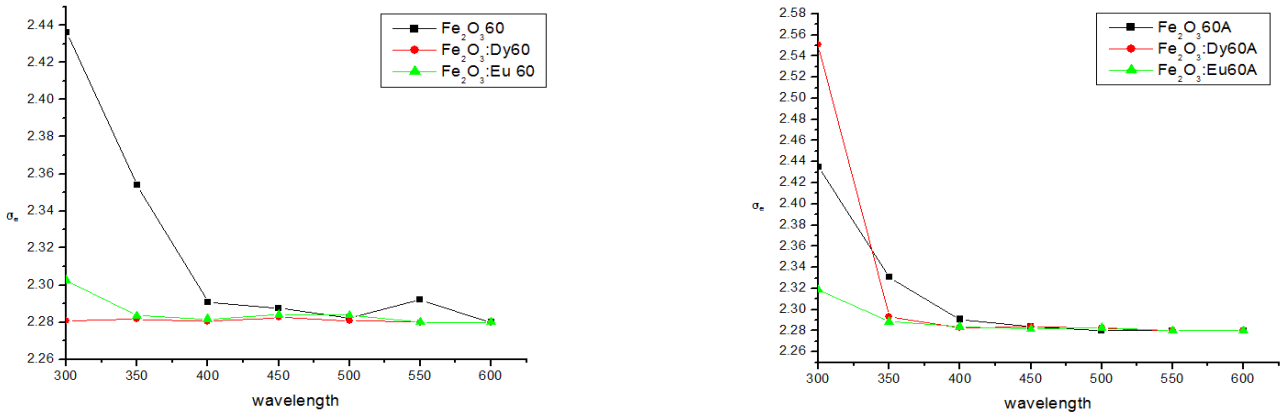


(a) un- annealed (b) annealed

Fig 6 (a) and (b) - Electrical Conductivity of $Fe_2O_3$ , $Fe_2O_3$ : Dy and $Fe_2O_3$ : Eu for 60 SILAR cycle on un- annealed and annealed film.

### 2.3.5 Real Dielectric Constants:-

Figures 7 (a) and (b) show the variation of real dielectric constants with wavelength of $Fe_2O_3$, $Fe_2O_3$ : Dy and $Fe_2O_3$ : Eu at 60 SILAR cycles for un-annealed and annealed films.

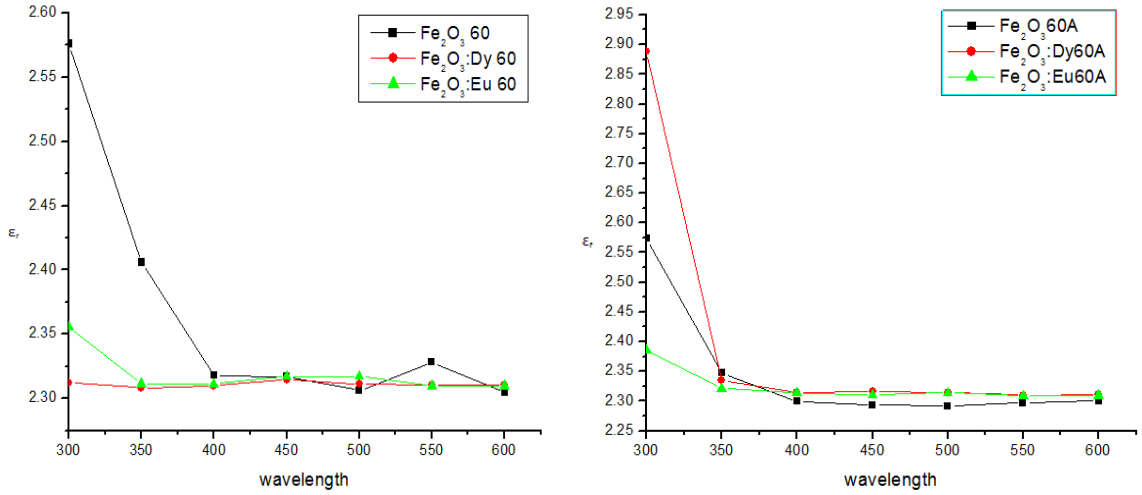


(a) un-annealed (b) annealed

Fig 7 (a) and (b) - Real Dielectric Constants of $Fe_2O_3$ , $Fe_2O_3$ : Dy and $Fe_2O_3$ : Eu for 60 SILAR cycle on un-annealed and annealed film.

### 2.3.6 Imaginary Dielectric Constants:-

Figures 8 (a) and (b) show the variation of imaginary dielectric constants with wavelength of $Fe_2O_3$, $Fe_2O_3$ : Dy and $Fe_2O_3$ : Eu at 60 SILAR cycles for un-annealed and annealed films.

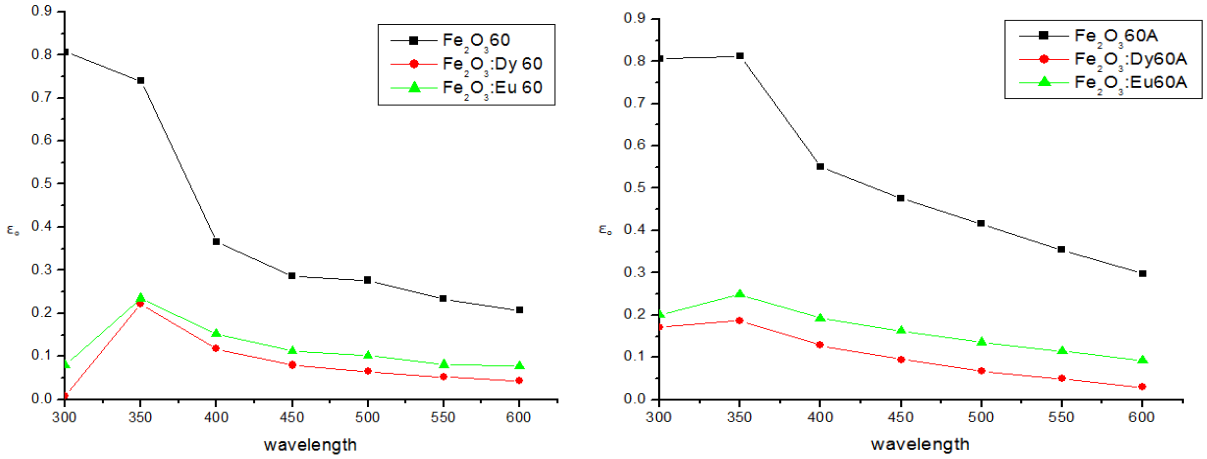


(a) un-annealed (b) annealed

Fig 8 (a) and (b) - **I**maginary Dielectric Constants of $Fe_2O_3$ , $Fe_2O_3$ : Dy and $Fe_2O_3$ : Eu for 60 SILAR cycle on un-annealed and annealed film.

A similar nature of variation of all these constants with wavelength has been observed. Pure $Fe_2O_3$ films had higher values of all the constants in comparison to the doped films. The implications of the variation of the optical constants for $Fe_2O_3$ films can be a subject of extensive study.

**Conclusion:** Pure and doped $Fe_2O_3$ thin films were deposited using SILAR method at 60 SILAR cycles. Rare earth elements Dy and Eu were used as do-pants. All the films were annealed at 300℃ after deposition. Optical absorption spectra was studied to determine the band gaps and also for calculation of optical constants. The band gap energy values were found to be in the range of 2.95eV to 3.15eV and the doped films showed higher band gap than the un-doped films. The band gap values were lower in the case of annealed films. The optical constants were plotted against wavelength and all the constants showed similar nature with higher values at lower wavelengths and constant in the entire range of the visible spectrum.

**References**

[1] A.U. Ubale, M.R. Belkhedkar, 2015.Size Dependent Physical Properties of Nanostructured α-$fe_2O_3$ thin films grown by successive ionic layer adsorption and reaction method for antibacterial application, J. Materials Science & Technology. 31(1), 1-9.

[2] S.H. Zhan, D.R.Chen, X.L. Jiao, S.S. Liu, 2007. General Strategy for Designing Functionalized Magnetic Microspheres for Different Bio-applications, J. Colloid Interface Sci.308 265-270.

[3] C. Jia, L. Sun, Z. Yan, L. You, F. Luo, X. Han, Y. Pang, Z. Zhang, C. Yan, Angew. 2005, Investigation on Magnetic Properties of hematite superstructures with controlled microstructures J. Chemical Engineering. 44,4328-4333.
[4] M. Cavas, R.K. Gupta, A.A. Al-Ghamdi, Z.H. Gafer, F. El-Tantawy, F. Yakuphanoglu, 2013. Preparation and characterization of dye sensitized solar cell based on nanostructured Fe2O3 J. Mater. Lett. 105, 106-109.
[5] M. R. Belkhedkar, A. U. Ubale, 2014. Preparation and Characterization of Nanocrystalline α-$Fe_2O_3$ Thin Films Grown by Successive Ionic Layer Adsorption and Reaction Method, 4(5): 109-116.

[6] M. Pelino, C. Colella, C. Cantalini, M. Faccio, G. Ferri, A. D'Amico.1992. Microstructure and electrical properties of an C–hematite ceramic humidity sensor, J. Elsevier 7, 464.

[7] H. Kitaura, K. Takahashi, F. Mizuno, A. Hayashi, K. Tadanaga, M. Tatsumisago, 2008. Mechanochemical synthesis of α-$Fe_2O_3$ nanoparticles and their application to all-solid-state lithium batteries, J. Power Sources, 183, 418.
[8] M. Frites, Y. A. Shaban, S. U.M. Khan, 2010. Iron oxide (n-Fe2O3) nanowire films and carbon modified (CM)-n-$Fe_2O_3$ thin films for hydrogen production by photosplitting of water, Int. J. hydrogen energy,35, 4944.
[9] J. H. Kennedy, D. J. Dunnwald, 2013. Photooxidation of organic compounds at α-Fe2O3 electrodes, J. Electro-chem. 130.
[10] Dean Cardillo, Konstantin Konstantinov, Thierry Devers ; ,2014. Synthesis and Characterization of Ce-doped α-$Fe_2O_3$ Nanoparticles for Ultraviolet Protection in Cosmetic Products, ResearchGate
[11] Ying Guoa,1, Tao Liua,1, Ning Wanga,b, Qiang Luoa, Hong Linc, Jianbao Lib, Qinglong Jiangd, Lili Wue, Zhanhu Guo. 2017. Ni-doped α-Fe2O3 as electron transporting material for planar heterojunction perovskite solar cells with improved efficiency, reduced hysteresis and ultraviolet stability, J. Elsevier, 38,193–200.
[12] M.R. Belkhedkar, A.U. Ubale, Y.S. Sakhare, Naushad Zubair, M. Musaddique. 2015. Characterization and antibacterial activity of nanocrystalline Mn doped Fe2O3 thin films grown by successive ionic layer adsorption and reaction method, J. of the Association of Arab Universities for Basic and Applied Sciences,
[13] Yichun Yin, Xiwang Zhang, Chenghua Sun. 2018. Transition-metal-doped Fe2O3 nanoparticles for oxygen evolution reaction, J. Elsevier, 28, 430–436.
[14] J. Sharmila Justus, S. Dawn Dharma Roy, A. Moses Ezhil Raj, 2016. Influence of Lanthanum Doping on the Structural and Optical Properties of Hematite Nanopowders, J. Applied Science and Engineering Methodologies. 2, 272-277.
[15] J. Park, M. Baek, E. Choi, S. Woo, J. Kim, 2009. Paramagnetic ultrasmall gadolinium oxide nanoparticles as advanced T1 MRI contrast agent: Account for large longitudinal relaxivity, optimal particle diameter, and in vivo T1 MR images, J. ACS Nano, 3, 3663–3669.
[16] Ceboliyozakha Leonard Ndlangamandla, Krish Bharuth-Ram, Osman Muzi Ndwandwe, Balla Diop Ngom, and Malik Maaza. 2015. Aqueous Synthesis of Ru Doped Hematite Nanostructures: A Morphological, Structural, Optical, and Magnetic Study J. Nanoparticles, 7.
[17] C. C. Chai, J. Peng, and B. P. Yan. 1996. Characterization of $\alpha$-Fe2O3 thin films deposited by atmospheric pressure CVD ontoalumina substrates, Sensors and Actuators, J. Chemical, 34, 1–3, 412–416.
[18]D. Sharma, S.Upadhayy, S. Choudhary, V. R. Satsangi, R. Shrivastav, and S. Dass. 2014. Enhancement of photoelectric conversion properties of $\alpha$-Fe2O3/Cu2O bilayered photoanode, International J. Materials, Mechanics and Manufacturing, 2, 1, 51–55.
[19]M.R. Belkhedkar, A.U. Ubale, Y.S. Sakhare, Naushad Zubair, M. Musaddique. 2015. Characterization and antibacterial activity of nanocrystalline Mn doped Fe2O3 thin films grown by successive ionic layer adsorption and reaction method, j.jaubas, 03.001.
[20]Glasscock, J.A., Barnes, P.R.F., Plumb, I.C., Bendavid, A., Martin, P.J. 2008. Structural, optical and electrical properties of undoped polycrystalline hematite thin films produced using filtered arc deposition. Thin Solid Films, 516, 1716–1724.

[21]Bhar, S.K., Mukherjee, N., Maji, S.K., Adhikary, B., Mondal, A. 2010. Synthesis of nanocrystalline iron oxide ultrathin films by thermal decomposition of iron nitroprusside: structural and optical properties. Mate. Res. Bull. 45, 1948–1953.
[22]R.Swanepoel. 1983. Determination of the thickness and optical constants of amorphous silicon" J. phys.E. 16,1214-1222.
[23]Manifacier J.C., Gasiot J. Fillard J.P. 1976. A simple method for the determination of optical constants n, h and the thickness of a weakly absorbing thin film" J. Phys. 9, 1002-1004.